Chen, Q., Archbold, M. D., Allsopp, D. W. E., 2009. Design of Ultrahigh-Q 1-D Photonic Crystal Microcavities. *IEEE Journal of Quantum Electronics*, 45 (3), pp. 233-239.

Official URL: http://dx.doi.org/10.1109/jqe.2008.2010835

Design of Ultrahigh-Q 1-D Photonic Crystal Microcavities

Qin Chen, Martin D. Archbold, and Duncan W. E. Allsopp, *Member, IEEE*

***Abstract*—Waveguide based 1-D photonic crystal (PC) microcavities in silicon-on-insulator are investigated by 2-D finite-difference time-domain method. Values up to 6.7×10^6 for the quality factor (Q) are feasible if the cavities are properly designed. The factors that govern Q are analyzed in both real space and momentum space. Etching down into the SiO_2 layer is found to give more than 20% improvement in Q compared to the structure in which etching is stopped at the oxide layer. Short air gap mirrors are used to reduce the vertical scattering loss. The addition to the Bragg mirrors of tapered periods optimized to produce a cavity mode with a near Gaussian shaped envelope results in a major reduction in vertical loss. A new tapered structure with varying Si block width demonstrates an ultrahigh-Q and relieves the fabrication constraints compared to the conventional air slots tapered structure.**

***Index Terms*—Filters, finite difference methods, microresonators, optical resonators, Q-factor.**

I. Introduction

PHOTONIC microcavities with ultrahigh quality factor (Q) and ultrasmall modal volume have great potential in the application of low threshold lasers [1], high finesse filters [2], single photon devices [3], nonlinear optics [4], and slow light [5]. The Q per modal volume (Q/V) is the defining characteristic of a resonant cavity. Normally a cavity with a smaller volume suffers more severely from radiation loss. Photonic band gaps, like the energy bandgap in semiconductors, opens up entirely new possibilities to achieve an ultrahigh Q/V. A localized defect state in a 3-D photonic crystal (PC) gives an infinite Q and a very small V. However, the fabrication of a 3-D PC in micro- or nano-scale is very difficult using present techniques. Major improvements in the Q of 2-D PC slab microcavities have been reported by several groups over recent years. Noda *et al.* experimentally demonstrated a resonant mode with a Q of 4.5×10^4 in a PC slab with air cladding by carefully tuning the holes close to the cavity and concluded that ultrahigh-Q is obtained if the envelope of the cavity mode fits a Gaussian field profile [6]. Kuramochi demonstrated a cavity based on a line defect with a loaded Q of 8.0×10^5 in a PC slab [7]. Recently, Noda further improved Q to 9.5×10^5 in their double-hetero-PC cavity in which the lattice constant was changed at the interfaces [8].

Manuscript received December 10, 2007; revised April 03, 2008. Current version published February 25, 2009. This work was supported the European Union under Framework 6 contract number 017481, STREP "N2T2."

The authors are with the Department of Electronic and Electrical Engineering, University of Bath, Bath BA2 7AY, U.K. (e-mail: Q.Chen@bath.ac.uk; mda23@bath.ac.uk; eesda@bath.ac.uk).

Digital Object Identifier 10.1109/JQE.2008.2010835

A 1-D PC cavity etched into an optical waveguide [9] is another interesting candidate for the high-Q resonant cavity. Compared to 2-D PC slab cavities with air claddings [6]–[8], 1-D PC cavity with a one-sided cladding structure possesses strong mechanical robustness and is thus attractive from the viewpoint of practical engineering. One main loss source is the etched air slots, where there is no refractive index contrast in the vertical direction. The out-of-plane scattering loss, either into the air or into the substrate, causes a serious degeneration of Q. In the earliest report on 1-D PC microcavities, Krauss *et al.* suggested the use of short air slots to suppress the scattering loss [10], but the measured Q values were just several hundreds [9]–[13], which are much lower than those of 2-D PC slab cavities. More recently, significant improvements have been reported. Velha *et al.* demonstrated a 1-D PC cavity with tapered reflectors on silicon-on-insulator (SOI) wafers and obtained a Q of 8.9×10^3 [14]. Using a Fabry–Perot model, they estimated that an intrinsic Q of 3.8×10^5 could be obtained in a cavity with two tapered semi-infinite mirrors. Pruessner observed a resonance with a Q of 2.7×10^4 in a 1-D PC with a long cavity on SOI wafer by using a 4-micron-deep Si etch [15]. Lalanne designed a 1-D PC cavity based on a 2-D SOI geometry using the Fourier-expansion method. By considering the impedance match and radiation recycling, these researchers obtained a single resonance with a theoretical Q as high as 3.4×10^4 together with 89% transmission in a nonperiodic mirror structure [16].

In this paper, we explore by the finite-difference time-domain (FDTD) method the effect of etch depth, Si filling ratio in mirrors and different kinds of taper on Q in 1-D PC microcavities of 2-D SOI geometry. In particular, it is shown that a Q value as high as 6.7×10^6 become possible if the mirror periods closest the cavity region are tapered in an optimal way. Momentum space analysis of the localized mode reveals that the improvement results from the tapers suppressing the amplitude of the wave vector components in the leaky region of the resonant mode, thereby suppressing the vertical radiation loss.

II. Method

SOI is emerging as an interesting platform for integrated nanophotonics due to the high refractive index contrast between the silicon core and the oxide cladding. This material system is very well suited for high density integration of photonic components and circuits which can be fabricated by standard CMOS technology.

Fig. 1 shows the basic structure used in the simulation work reported here. It comprises a block of SOI material consisting of a Si substrate, SiO_2 buffer layer of 1.5 μm, the top Si guide

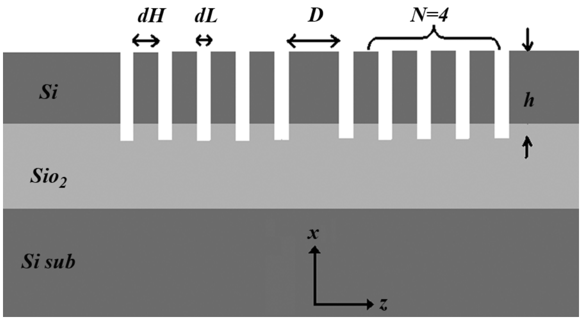

Fig. 1. Schematic of a 1-D PC cavity on SOI material with 4 pairs of Si/air mirrors.

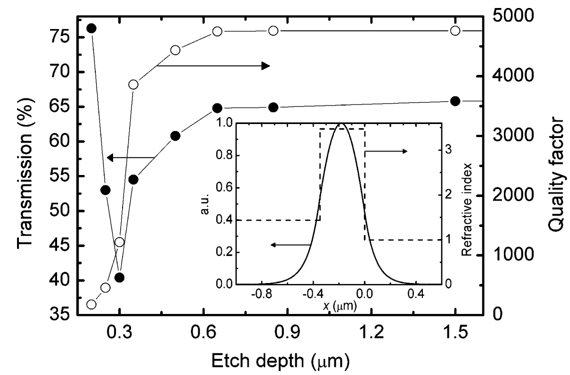

Fig. 2. Transmission on resonance and Q versus the etch depth of mirrors, where $D = 400$ nm, $dH = 200$ nm and $dL = 90$ nm. The field distribution of the vertical four-layer slab waveguide is shown in the inset.

layer of 360 nm and the air cladding layer. The refractive indexes of silicon and silicon dioxide are 3.48 and 1.46, respectively. It is assumed that a central cavity layer is then formed by etching Bragg mirrors, each comprising N pairs of Si and air gap layers. In the 2-D FDTD simulations, the corrugated waveguide is assumed to be illuminated from the input waveguide by the transverse magnetic (TM, $H_y = 0$) fundamental mode, which is a Gaussian-modulated cosine impulse covering a wide frequency band [17]. The "bootstrapping" technique is used to set the exciting source [17]. The perfectly matched layer (PML) absorbing boundary is used to terminate the FDTD calculation window, with the PML thickness of 0.5 and 1 μm in the x and z directions, respectively. The spatial cell size is 10 nm, and the time step is Courant limit [17]. The transmission spectra are calculated from the power flux recorded at the detector plane, which is normalised by the source value [18]. The resonance wavelength is found by fitting a Lorentzian to the transmission peak and Q is given by the ratio of the peak wavelength to its 3-dB bandwidth.

By compressing the incident impulse spectral width into a range narrow enough to ensure that only on-resonance modes can be excited, we can obtain the mode field distributions from the FDTD simulation. The spatial Fourier transformation spectra, which represent the plane wave components of the cavity mode, are then calculated from these field distributions.

The analysis is valid for 1-D PC structures in 2-D cross section geometry, which is an approximation to the actual 3-D structures. In the case of air slots without transverse waveguide confinement, our 2-D model neglects the scattering loss in the third dimension, i.e., Q reported here is the upper limit. In practice, the width of the access waveguide must be finite, even tapered [13], to ensure single mode behavior in the PC cavity part and low insertion loss at each end of the device.

III. Cavities With Short Air Gap Bragg Mirrors

The basis of the simulations is a 1-D PC microcavity with each reflector comprising 8 pairs of Bragg mirrors. Instead of quarter wave stacks, high Si filling ratio (defined as $dH/(dH + dL)$) mirrors are used to realize light confinement and suppress scattering losses at the interface between Si blocks and air slots [10].

A. Etch Depth

The etch depth of the air slots is an important factor. Deep gratings are expected to exhibit strong Bragg reflection effect, while in practical device fabrication small feature sizes can limit the etch depth via the aspect ratio dependent etching [19]. Fig. 2 shows the variation of the transmission at resonance and Q with etch depth, h, at $dH = 200$ nm, $dL = 90$ nm, and $D = 400$ nm. Q increases sharply as the etch depth into the Si guiding layer increases, then rises more slowly as the air gap penetrates into the underlying SiO_2 layer and finally saturates for $h > 650$ nm. This behaviour occurs because the confinement of the cavity mode in a weakly corrugated waveguide is much lower than that in an etched-through structure where the refractive index contrast is larger.

The inset of Fig. 2 shows the approximate vertical field distribution in the device, from which the effect of the etch depth, h, of the air slots on microcavity performance can be deduced. Since the cavity mode evolves from the slab modes of the air–Si–SiO_2 feeder waveguides, it will have a similar vertical field distribution. For the very shallow air slots, the mode mismatch between the input waveguide and the microcavity is small and the transmission is still high. Increasing the etch depth, the mismatch increases and the scattering loss increases with the increasing index contrast [20].

On resonance transmission undergoes a rapid variation with h as a result of two effects. Light couples from the input waveguide either via butt-coupling of the dielectric waveguide formed by any residual dielectric layers under the air gap or via near-field radiation from the effective aperture formed by end facet created by the air gap. The contribution from waveguide coupling is governed by the overlap integral of the two waveguide modes. This decreases with increasing h, reaching a minimum when the residual waveguide is cut-off. At the same time the area of the effective aperture formed by the facet formed by the air gap increases linearly with increasing h and radiative coupling ultimately dominates. Such radiative coupling saturates when the air gap extends beyond the extent of the guided mode illuminating the facet. The crossover is expected to occur when the residual waveguide below the air gap approaches cut off. This explains qualitatively the behaviour of $T_{\rm res}$ in Fig. 2.

High Q requires high reflectivity mirrors. For short Bragg reflectors, this requirement is met by maximising the effective dielectric contrast at the interfaces between the low and high index sections. Having deep air slots increases the effective dielectric contrast, defined as $[h\varepsilon_{\text{air}} - (H-h)\varepsilon_{\text{mode}})]/\varepsilon_{\text{mode}}$ where H is the full height of the Si waveguide core and $\varepsilon_{\text{mode}}$ is the modal index for slab mode propagation in the Si blocks of a PC period. Therefore, increasing h gives rise to a rapid increase in Bragg reflection and hence Q. Once the air gap is sufficiently deep to extend over the full range of the vertical mode profile there is no further increase in T_{res} and Q. Overall, deep air slots give the highest dielectric contrast and thus give the largest Q and simultaneously a high transmission.

B. Si Filling Ratio in the Reflector

Varying the Si filling ratio in the reflector changes the reflectivity and relative phase, which affect Q and the resonant wavelength. In Fig. 3, Q and wavelength are shown as functions of Si filling ratio, where $D = 400$ nm, $h = 650$ nm, dH and dL are changed around central values of 200 and 90 nm, respectively.

At a fixed air gap length as in Fig. 3(a), the resonance wavelength is found to increase almost linearly with the Si filling ratio, where the effective light propagation distance in one period of mirrors increases linearly with the increasing width of Si blocks. When changing the width of air slots at a fixed width of Si blocks, a similar relation is observed in Fig. 3(b), where a decrease of Si filling ratio means an increase in the width of air slots and effective light propagation. In both cases, the resonance wavelength is very sensitive to the widths of air and silicon blocks used in the mirrors, for example, a systematic 10 nm fabrication error in the width of Si blocks will cause a 20 nm offset in the resonance wavelength.

In practical device fabrication, the period $dH + dL$ is in effect fixed and both types of error will occur owing to limited processing tolerances. This situation is considered in Fig. 3(c) where $dH+dL$ is fixed at 290 nm and both dH and dL are varied for Si filling ratios around 0.7 (achieved when $dH = 200$ nm, $dL = 90$ nm). Now the resonant wavelength, λ_{res}, shows a variation of only 2 nm, essentially fixed at 1.67 μm, over a range of Si filling ratios that corresponds to a ± 20 nm fabrication error. This demonstrates that λ_{res} is a robust parameter in 1-D PC microcavity design and fabrication although Q is more dependent on process tolerances. Compared to the optimum for $\lambda_{\text{res}} = 1.67$ μm, a smaller Si filling ratio results in larger scattering loss at the interface between Si blocks and air slots, whilst a larger ratio results in lower reflection by the reflectors, both effects reducing Q.

C. Cavity Length

Transmission and Q are calculated with different cavity length D as shown in Fig. 4. Around $D = 400$ nm, transmission increases from $D = 340$ nm to 460 nm and Q has a maximum at $D =\sim 360 - 370$ nm. When D increases, the resonance moves close to the bandgap edge and suffers more loss. When D decreases, transmission disappears. Therefore, there is a tradeoff when choosing the cavity length. In later sections, D is set to be 400 nm, which supports both reasonable high transmission and Q.

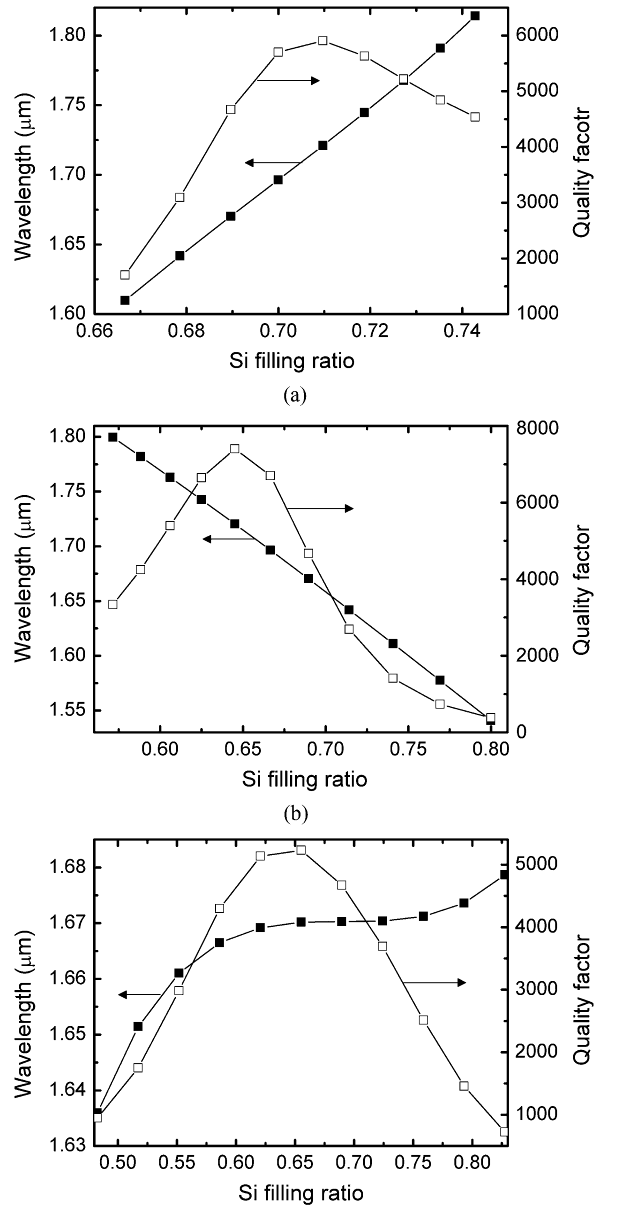

Fig. 3. Resonance wavelength and Q versus Si filling ratio in the reflectors. (a) dH is stepped in the sequence 180, 190, ..., 260 nm, dL = constant = 90 nm. (b) dH = constant= 200 nm, dL stepped in the sequence 50, 60, ..., 150 nm. (c) dH stepped in the sequence 140, 150, ..., 240 nm, $dH + dL$ = constant = 290 nm.

D. Number of Mirror Periods

Fig. 5 shows the transmission and Q as functions of the number, N, of mirror pairs for a structure of the generic type shown in Fig. 1. The variation of Q can be divided into three stages. Firstly, Q increases exponentially when N is less than 10. Secondly, it increases slowly from $N = 10$ to 16. Thirdly, it becomes saturated when N is larger than 16.

In a 2-D model of a 1-D PC cavity in SOI slab waveguide as shown in Fig. 1, there are two loss mechanisms. One is the longitudinal radiation loss, which depends on the degree of light confinement due to the Bragg mirrors, and the other is the vertical radiation loss caused by the mode coupling between the resonant mode in the cavity and the radiation mode in the cladding

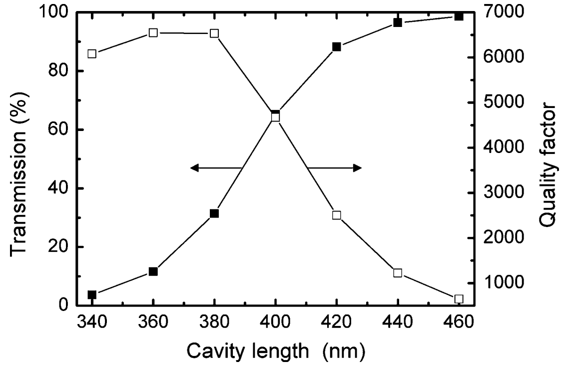

Fig. 4. Transmission and Q versus the cavity length, where h = 650nm, dH = 200 nm and dL = 90 nm. On resonance wavelengths are also shown.

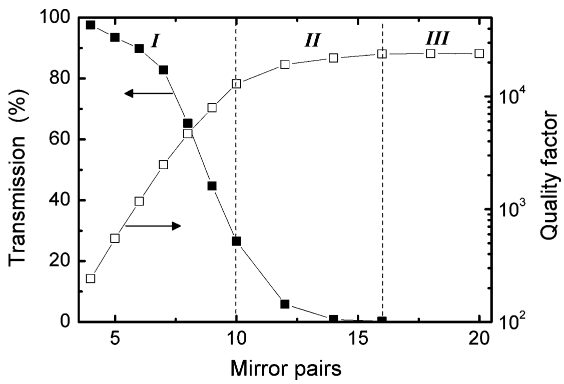

Fig. 5. Transmission and Q versus mirror pairs N, where dH = 200 nm, dL = 90 nm, D = 400 nm, and h = 650 nm.

layer. With two such loss mechanisms, the Q of a 1-D PC microcavity can be given by

$$\frac{1}{Q} = \frac{1}{Q_L} + \frac{1}{Q_V}. \tag{1}$$

In (1) Q_L and Q_V are the values the quality factor would take if, respectively, longitudinal loss or vertical loss were the sole degradation mechanism. Since Q_L behaves in a similar way to the conventional loss mechanisms in a Fabry–Perot resonator, it will increase exponentially with increasing number, N, of mirror periods whereas the longitudinal confinement has only a slight effect on Q_V. Therefore, for small N the longitudinal loss dominates the total loss, i.e., $Q_L \ll Q_V$ and, from (1), $Q \approx Q_L$. This corresponds to region I of the dependence of Q on N shown in Fig. 5. With an increase in N, the longitudinal and vertical loss become comparable, i.e., $Q_L \approx Q_V$, and have almost the same effect on Q, region *II* of Fig. 5. With further increase in N, the vertical loss becomes dominant, i.e., $Q_L \gg Q_V$, and Q saturates a value limited by Q_V, region *III* of Fig. 5.

From Fig. 5, Q_V is found to be about 2.4×10^4. No matter how many mirrors are located at each side of the central cavity, Q can not be larger than Q_V. Obviously, this is much lower than those observed in 2-D PC cavities [8]. Transmission is found to decrease quickly with N. The main reason is the increase of the out-of-plane scattering loss from the mirror interfaces induced by the additional mirrors [20], [21]. Increasing reflection also contributes to the decrease of the transmission. As shown in Fig. 5, greater than 50% of incident power is scattered out when N is larger than 8. If this cavity is used as a filter, a tradeoff between transmission and Q has to be considered.

E. Momentum Space Analysis

As in 2-D PC slab cavities, 1-D PC cavities with periodic structures in one direction do not have a complete photonic band gap. The light confinement is realized by total internal reflection in the two other directions. The localized mode in the cavity can be seen as a combination of numerous plane wave components with wave vectors k, which may couple with the radiative modes in the cladding layer. The inevitable vertical radiation loss prevents the ultrahigh-Q resonance. The mode field in such a structure can be written as:

$$F(x,z) = f(x,z)e^{-ik_x x}e^{-ik_z z} \tag{2}$$

$$k_x^2 + k_z^2 = k^2 = \left(\frac{2\pi}{\lambda}\right)^2 \tag{3}$$

where k_x and k_z are the vertical and tangential components of wave vector k, and λ is the resonant wavelength. If k_z lies within the range $0 - 2\pi/\lambda$, k_x is a real number, which means the mode is not confined in the vertical direction. All plane wave components having k_z in the range of $0 - 2\pi/\lambda$ (called the leaky region below) result in the vertical loss of the resonant mode. The spatial Fourier transform (SFT) of the longitudinal field distribution provides the spectral distribution of its plane wave components and enables analysis of the vertical loss [6], [22].

Fig. 6 shows the electric field distribution of the resonant mode in the longitudinal direction in 1-D PC microcavities for $N = 8$ and $N = 16$. The dotted lines in Figs. 6(a) and 6(b) indicate the position of the central cavity relative to the mode field profiles. As Fig. 6(a) reveals, the longitudinal field of the cavity mode is antisymmetric with respect to a vertical symmetry plane through the centre of the cavity.

Although the Q of the microcavity formed by $N = 16$ mirrors, at 2.4×10^4, is ~ 5 times higher than that with $N = 8$ mirrors, the normalized integral of the spectral intensity over the leaky regions of the SFTs are 2.2×10^{-3} and 1.5×10^{-3} for N =8 and 16, respectively. This indicates a reduction of only $\sim$ 1.5 times in the vertical loss by 8 additional mirror pairs. This is reasonable because the electric field profile around the central cavity in the longitudinal direction shows no obvious change with the increase in the number of mirror periods, as can be seen in Fig. 6(b). The slightly higher integrated spectral intensity in the leaky region for the $N = 8$ structure, compared to that of the $N = 16$ device, derives from its different electric field distribution at the outer edge of the reflectors. The stronger electric field variation at the boundary of the whole structure at $N = 8$ introduces an additional vertical radiation loss.

IV. Cavities With Tapered Mirrors

In 2-D PC microcavity technology, tailoring the positions of the holes around the cavity is a proven method for achieving ultrahigh Q by suppression of spectral components of the resonant mode lying in the leaky region of momentum space [8]. The theoretically optimum shape for the field envelope of the resonant

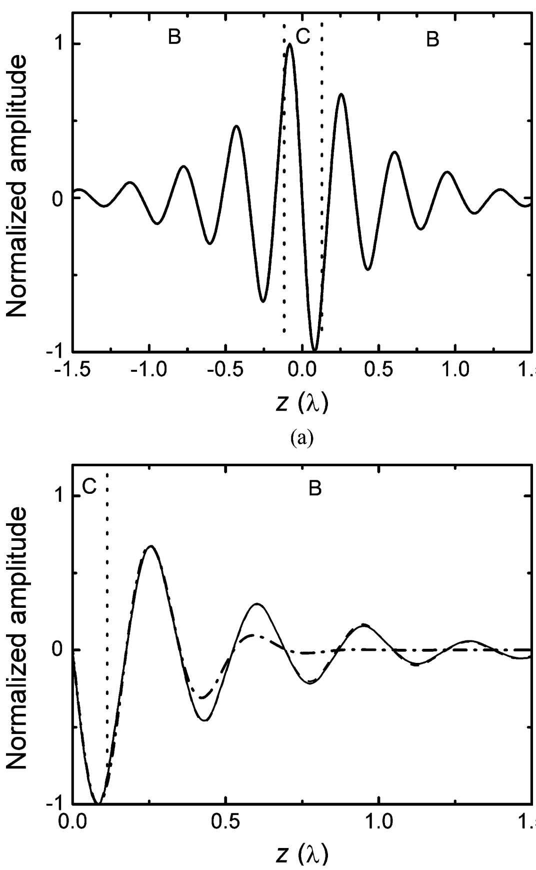

Fig. 6. Electric field profile (solid line) at the boundary between the top Si layer and the oxide buffer layer in a 1D PC cavity for (a)N =8 and (b) N = 16, other parameters are the same as those in Fig. 5. The fitting curve obtained by Gaussian envelope function for) 16 and the right half of the profile in (a) are plotted in (b) as a dash dot line and a dashed line for comparison. "B" and "C" separated by the dot line indicate Bragg mirrors and the central cavity.

mode is a *sinc* function as its SFT is rectangular and can be engineered not to overlap with the leaky range of k_z components. A Gaussian shaped envelope has been shown to be a practical alternative, requiring less rigorous optimization [6], [8]. It is shown here that mirror pairs with tapering variations in their periodicity fulfil the same role in increasing Q by creating a nearly Gaussian shaped envelope for the cavity mode in 1-D PC microcavities as optimal holes positioning have in 2-D structures.

A. Linearly Varying Air Gap Tapers

Linearly tapered air slots are discussed in this section, where the minimum value of air gap considered is 50 nm, a limit beyond which fabrication becomes difficult. Tapers are added to the Bragg reflectors by reshaping the four air slots in each mirror closest to the central cavity layer so that their widths increase from 50 to 80 nm, in steps of 10 nm, moving away from the cavity while the Si section lengths remain constant. Fig. 7 shows the variations in Q (open squares) and transmission (solid squares) with the total number of mirror periods, N. The variations in Q and transmission with N follows the trends shown in Fig. 5, except that the saturated value of Q, i.e., Q_V,

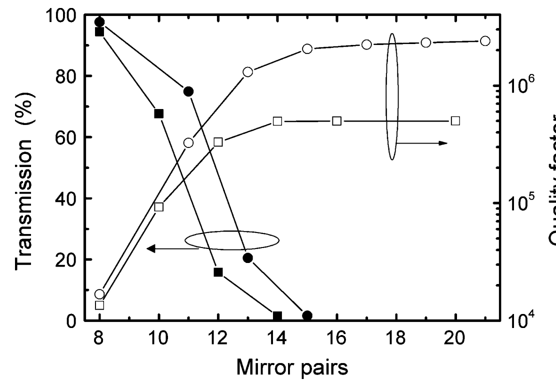

Fig. 7. Transmission and Q versus the number of mirror pairs in a 1D PC microcavity with linearly (square symbols, four air slots close to the central Si cavity at each side are 50, 60, 70, 80 nm wide) and nonlinearly (circular symbols, three air slots close to the central Si cavity at each side are 50, 70, 80 nm wide) tapered mirrors. Other parameters are the same as those in Fig. 5.

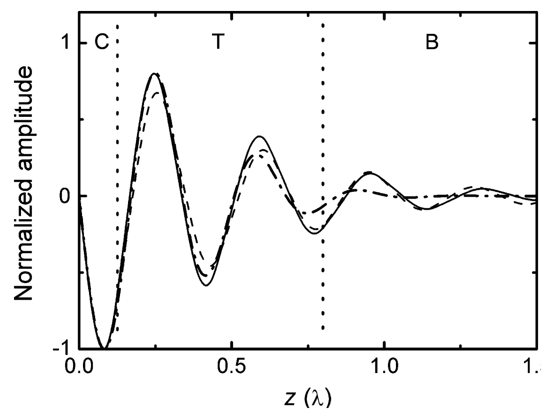

Fig. 8. Electric field profile (solid line) at the boundary between the top Si layer and the oxide buffer layer in a 1D PC cavity with linear tapers for N = 14, other parameters are the same as those in Fig. 7. The fitting curve obtained by Gaussian envelope function and the electric field profile in the nontapered structure at $N = 16$ [Fig. 6(b)] are plotted as a dash dot line and a dashed line for comparison. The regions labeled "B," "T," and "C" and delineated by the dotted lines indicate the positions of the normal Bragg mirrors, tapers and the central cavity relative to the mode field (only distribution at the half region $z > 0$ are plotted).

has increased significantly from 2.4×10^4 in Fig. 5 to 5.0×10^5 with the introduction of tapers.

The electric field variation in the longitudinal direction is shown in Fig. 8 for the linearly tapered 1-D PC cavity at $N = 14$. Due to the antisymmetric property of the mode profile, only the distribution in a half region $z > 0$ is plotted for clarity. The electric field profile (solid line) around the central cavity in the tapered structure agrees well with the fitting curve obtained by Gaussian envelope function (dash dot line). On the other hand, the electric field profile in a nontapered structure (dashed line) shows a marked departure from the Gaussian profile, notably over the normalized distance $0.2\lambda \leq z \leq 0.5\lambda$. The normalized integral of the difference between the electric field profile and the Gaussian fitting curve is about 0.6% in the region of $-0.5\lambda \sim 0.5\lambda$ for the linearly tapered structure for $N = 14$, however, it is as high as 4.7% in the nontapered structure for $N = 16$. It can be seen that the electric field profile now changes more gently around the central cavity than it does in the nontapered structure to reduce the vertical loss.

This is verified by the normalized integral of the spectral intensity in the leaky region of SFTs, which are 1.3×10^{-4} and 8.9×10^{-5} in the tapered structure for $N = 8$ and $N = 14$, respectively, a $\sim$ 20-times suppression of vertical radiation loss compared to the nontapered structure. Although the $Q(1.3 \times 10^4)$ of the $N = 8$ tapered microcavity is less than that of the $N = 16$ cavity without tapers considered in Fig. 6(b), it is now limited by longitudinal loss and hence by Q_L rather by Q_V as in the case of the latter. The reduction of the intensity of the wave vector components in the leaky region, indicates a method to obtain an ultrahigh Q via increases in Q_V by the use of tapers. For example, Q values as high as 7.4×10^5 result from incorporating linear tapers with 50, 70, and 90 nm air slots increasing from the cavity edge towards the unperturbed mirrors.

For both linearly varying air gap tapers considered in this section, the transmission is significantly improved compared to the nontapered structures with the same number of mirror pairs. However, transmission still drops rapidly with increasing number of mirror pairs.

B. Nonlinear Tapers

Whilst Bloch wave engineering offers a design method for increasing the transmission [16], it is shown here that nonlinear tapers provide a flexible alternative to optimize the field profile around the boundary of the central cavity in order to match the desired Gaussian profile. Even higher Q, around 2.4×10^6, is obtained in a structure with three pairs of tapered mirrors at each side, i.e., dL_{1-3} =50, 70, 80 nm, where dL_i is the width of the $i'\mathrm{th}$ air gap numbered from the central cavity, together with 16 pairs of periodic mirrors. A 100 times improvement is obtained compared to the nontapered structure. The whole cavity length is around 7λ including the reflectors. Transmission and Q versus mirror pairs are shown as circular symbols in Fig. 7. The transmission also improves significantly, with the nonlinear tapers making theoretically possible a 1-D PC microcavity with $Q > 3 \times 10^5$ with 75% transmission.

C. Si Blocks Tapers

As discussed above and in [11], [12], tapers are usually formed by systematically reducing the width of the air slots. This creates a problem in practical device fabrication arising from the impact of aspect ratio dependent etching of the narrower air slots [19]. If instead the air slots in the tapers are kept the same as in the normal periodic mirrors (in this work 90 nm) and the widths of the Si blocks now are tailored to match the field profile with the Gaussian function, the fabrication constraints are eased. This is due to the optimum width of the Si block in a PC period being larger than the air gap.

If the widths of just the first Si block on each side of the central layer are reduced from 200 to 180 nm, Q_V increases to 6.4×10^5. If two mirror periods are altered so that in each Bragg reflector the two Si blocks closest to the central cavity are 170 and 180 nm, respectively, a Q of 9.8×10^5 is obtained. A Q as high as 6.7×10^6 is obtained when the widths of the three Si blocks in each reflector closest to the central cavity are 170, 180, and 190, nm respectively. To the best of our knowledge, this is the record predicted value for a 1-D PC microcavity

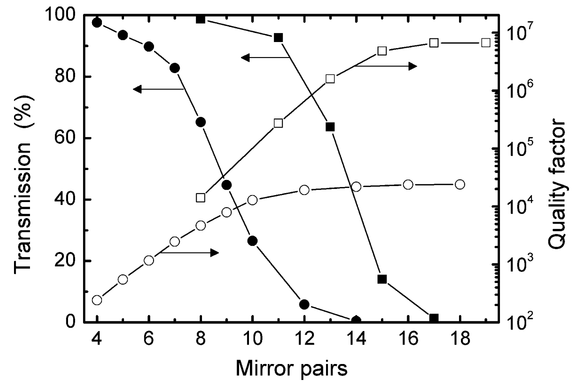

Fig. 9. Transmission and Q versus mirrors pairs in a 1-D PC microcavity with Si block tapers. The tapers are formed by, on each side, adjusting the widths of the three Si blocks closest to the central Si cavity to 170, 180, 190 nm increasing towards to unmodified Bragg reflectors whilst keeping the air gap widths constant.

from a 2-D FDTD model. Transmission and Q for this 3 period variable width Si block fixed air gap taper are shown as functions of the mirrors pairs in Fig. 9. Compared to the nontapered structure, both transmission and Q show a major improvement. The transmission of a resonance with a Q above 10^6 is larger than 70% and that with a Q above 10^5 is above 90%, which is ideal for applications in nonlinear optics. At the same time, structures with nontapered air slots are much easier fabricated since the minimum feature size can now be as large as 90 nm.

V. Modal Area

Finally, the modal area S in the 2-D model can be used as an alternative to modal volume V in order to investigate the variation of mode size due to the cavity reshaping. Similar to the definition of V in [1], S can be written as

$$S = \frac{\int \varepsilon(\boldsymbol{r}) \left|E(\boldsymbol{r})\right|^2 d^2\boldsymbol{r}}{\max(\varepsilon(\boldsymbol{r}) \left|E(\boldsymbol{r})\right|^2)} \tag{4}$$

where $E(\boldsymbol{r})$ is the electric field profile, $\varepsilon(\boldsymbol{r})$ is the dielectric constant and $\boldsymbol{r}$ is the position vector. The calculated modal area for the $N = 16$ untapered cavity with the mode envelope shown in Fig. 6(b) and the nearly equivalent $N = 17$ structure with tapered Si blocks (Fig. 9) are 0.1205 and 0.1263 $\mu\mathrm{m}^2$, respectively. The cavity tailoring improves Q by around 300 times but keeps the mode volume almost constant, giving rise to almost equivalent improvement in Q/V.

VI. Conclusion

In conclusion, the FDTD method has been used to demonstrate how the structure of a SOI 1-D PC microcavity can be optimized to support an ultrahigh Q resonance yet retain acceptably high transmission. Using a 2-D model, it is shown how tapers inserted between the central cavity section and the Bragg reflectors can be used to shape the envelope of the resonant mode to minimize the vertical radiation loss. Analysis of the spatial Fourier transform of the cavity field has revealed that the tapers have much the same effect as optimizing the positions of the holes in 2-D PC SOI microcavities in reducing the intensity of leaky spectral components of the resonant mode.

In particular, two new forms of taper are considered, both of which result in predicted Q of greater than 2×10^6. The first comprises three PC periods in which the Si block width is kept constant whilst the air slots are increased nonlinearly from the central section of the cavity towards the Bragg reflectors. The second comprises tapers are formed by optimizing the widths of the first three Si blocks in each mirror nearest the central section whilst keeping the air slots constant. The latter approach yielded a resonance with Q as high as 6.7×10^6. The same basic structure can be detuned by using fewer PC periods in the reflectors to achieve simultaneously theoretical Q approaching 1×10^6 with $> 70\%$ transmission. Whilst the 3-D nature of any practical 1-D PC microcavity of the type considered here will lead inevitably to lower Q in practice, the design features for simultaneous high Q and high $T_{\rm res}$ revealed by the 2-D FDTD modeling reported here are expected to be robust.

REFERENCES

[1] O. Painter, R. K. Lee, A. Scherer, A. Yariv, J. D. O'Brien, P. D. Dapkus, and I. Kim, "Two dimensional photonic bandgap defect mode laser," *Science*, vol. 284, pp. 1819–1821, 1999.

[2] S. Noda, A. Chutinan, and M. Imada, "Trapping and emission of photons by a single defect in a photonic bandgap structure," *Nature*, vol. 407, pp. 608–610, 2000.

[3] P. Michler, A. Kiraz, C. Becher, W. V. Schoenfeld, P. M. Petroff, L. Zhang, E. Hu, and A. Imamoğlu, "A quantum dot single-photon turnstile device," *Science*, vol. 290, pp. 2282–2285, 2000.

[4] Q. Xu, B. Schmidt, S. Pradhan, and M. Lipson, "Micrometre-scale silicon electro-optic modulator," *Nature*, vol. 435, pp. 325–327, 2005.

[5] T. Tanabe, M. Notomi, E. Kuramochi, A. Shinya, and H. Taniyama, "Trapping and delaying photons for one nanosecond in an ultrasmall high-Q photonic-crystal nanocavity," *Nature Photon.*, vol. 1, pp. 49–52, 2007.

[6] Y. Akahane, T. Asano, B. Song, and S. Noda, "High-Q photonic nanocavity in a two-dimensional photonic crystal," *Nature*, vol. 425, pp. 944–947, 2003.

[7] E. Kuramochi, M. Notomi, S. Mitsugi, A. Shinya, and T. Tanabe, "Ultrahigh-Q photonic crystal nanocavities realized by the local width modulation of a line defect," *Appl. Phys. Lett.*, vol. 88, p. 041112, 2006.

[8] T. Asano, B. Song, Y. Akahane, and S. Noda, "Ultrahigh-Q nanocavities in two-dimensional photonic crystal slabs," *IEEE J. Sel. Topics Quantum Electron.*, vol. 12, no. 6, pp. 1123–1134, Nov./Dec. 2006.

[9] J. S. Foresi, P. R. Villeneuve, J. Ferrera, E. R. Thoen, G. Steinmeyer, S. Fan, J. D. Joannopoulos, L. C. Kimerling, H. I. Smith, and E. P. Ippen, "Photonic-bandgap microcavities in optical waveguides," *Nature*, vol. 390, pp. 143–145, 1997.

[10] T. E. Krauss and R. M. De La Rue, "Optical characterization of waveguide based photonic microstructures," *Appl. Phys. Lett.*, vol. 68, pp. 1613–1615, 1996.

[11] M. Palamaru and P. Lalanne, "Photonic crystal waveguides out-of-plane losses and adiabatic modal conversion," *Appl. Phys. Lett.*, vol. 78, pp. 1466–1468, 2001.

[12] D. Peyrade, E. Silberstein, P. Lalanne, A. Talneau, and Y. Chen, "Short Bragg mirrors with adiabatic modal conversion," *Appl. Phys. Lett.*, vol. 81, pp. 829–831, 2002.

[13] A. S. Jugessure, P. Pottier, and R. M. De La Rue, "One dimensional periodic photonic crystal microcavity filters with transition mode matching features embedded in ridge waveguides," *Electron. Lett.*, vol. 39, pp. 367–368, 2003.

[14] P. Velha, J. C. Rodier, P. Lalanne, J. P. Hugonin, D. Peyrade, E. Picard, T. Charvolin, and E. Hadji, "Ultra-high-reflectivity photonic-bandgap mirrors in a ridge SOI waveguide," *New J. Phys.*, vol. 8, p. 204, 2006.

[15] M. W. Pruessner, T. H. Stievater, and W. S. Rabinovich, "Integrated waveguide Fabry–Perot microcavities with silicon/air Bragg mirrors," *Opt. Lett.*, vol. 32, pp. 533–535, 2007.

[16] P. Lalanne and J. P. Hugonin, "Bloch wave engineering for high-Q, small-V microcavities," *IEEE J. Quantum Electron.*, vol. 39, no. 11, pp. 1430–1438, Nov. 2003.

[17] A. Taflove*, Advances in Computational Electrodynamics: The Finite-Difference Time-Domain Method*. Boston, MA: Artech House, 1998, vol. 13, pp. 561–612.

[18] Q. Chen, Y.-D. Yang, and Y.-Z. Huang, "Distributed mode coupling in microring channel drop filters," *Appl. Phys. Lett.*, vol. 89, p. 061118, 2006.

[19] C.-K. Chung, "Geometrical pattern effect on silicon deep etching by an inductively coupled plasma system," *J. Micromech. Microeng.*, vol. 14, pp. 656–662, 2004.

[20] H. Bensity, C. Weisbuch, D. Labilloy, M. Rattier, C. J. M. Smith, T. F. Krauss, R. M. De La Rue, R. Houdré, U. Oesterle, C. Jouanin, and D. Cassagne, "Optical and confinement properties of two-dimensional photonic crystals," *J. Lightw.Technol.*, vol. 17, no. 11, pp. 2063–2077, Mar. 1999.

[21] S. Blair and J. Goeckeritz, "Effect of vertical mode matching on defect resonances in one-dimensional photonic crystal slabs," *J. Lightw. Technol.*, vol. 24, no. 3, pp. 1456–1461, Mar. 2006.

[22] K. Srinivasan and O. Painter, "Momentum space design of high Q photonic crystal optical cavities," *Opt. Exp.*, vol. 10, pp. 670–684, 2002.

Qin Chen received the B.Sc. degree in physics from Wuhan University, Wuhan, China, in 2001, and received the Ph.D. degree in microelectronics and solid state electronics from Institute of Semiconductors, Chinese Academy of Sciences, Beijing, China, in 2006. His Ph.D. research work focused on the microlasers and microresonant filters.

Since 2007, he has been working as a research officer in Department of Electronic and Electrical Engineering in University of Bath, Bath, U.K. His research interests include nanoimprint technology, design and fabrication of microresonator and photonic crystal devices.

Martin D. Archbold received the M.Sci. degree in Physics from Imperial College London, U.K., in 1999 and the Ph.D. degree in the field of thin film photovoltaic devices from the University of Durham in 2007.

Since 2007 he has been working in the Department of Electronic and Electrical Engineering, University of Bath, Bath, U.K., as a Research Officer. His research interests include photonic crystal device structures, nanoimprint technology, and porous alumina nanotemplate fabrication.

Duncan W. E. Allsopp (M'89) received the B.Sc. degree in physics and the M.Sc. and Ph.D. degrees from the University of Sheffield, Sheffield, U.K., in 1971, 1974, and 1977, respectively.

From 1977 to 1979, he was with Ferranti Electronics, Ltd., developing high-speed Si bipolar transistors. From 1979 to 1984, he was with the University of Manchester Institute of Science and Technology, Manchester, U.K., researching defects in semiconductors, and from 1984 to 1986, he was with British Telecom Research Laboratories, Martlesham Heath, U.K. In 1986, he joined the University of York, York, U.K., where he established a group researching photonic devices. Since 1999, he has been in the Optoelectronics Group, University of Bath, Bath, U.K., where he is currently a Royal Academy of Engineering/Leverhulme Trust Senior Research Fellow, where he continues his research into photonics.